Journal of Biomechanics xxx (xxxx) xxx

Contents lists available at ScienceDirect

Journal of Biomechanics

journal homepage: www.elsevier.com/locate/jbiomech
www.JBiomech.com

Determining the impacts of venoarterial extracorporeal membrane oxygenation on cerebral oxygenation using a one-dimensional blood flow simulator ☆

Bradley Feiger [a], Ajar Kochar [b], John Gounley [a,c], Desiree Bonadonna [d], Mani Daneshmand [e], Amanda Randles [a,*]

[a] Department of Biomedical Engineering, Duke University, Durham, NC, USA
[b] Department of Medicine, Duke University, Durham, NC, USA
[c] Computational Sciences and Engineering Division, Oak Ridge National Laboratory, Oak Ridge, TN, USA
[d] Duke University Medical Center, Durham, NC, USA
[e] Division of Cardiovascular and Thoracic Surgery, Duke University, Durham, NC, USA

ARTICLE INFO

Article history:
Accepted 23 February 2020
Available online xxxx

Keywords:
ECMO
1D blood flow
Computational fluid dynamics
Hemodynamics
Mixing zone

ABSTRACT

Venoarterial extracorporeal membrane oxygenation (VA-ECMO) is a mechanical system that provides rapid and short-term support for patients with cardiac failure. In many patients, pulmonary function is also impaired, resulting in poorly-oxygenated cardiac outflow competing against well-oxygenated VA-ECMO outflow, a condition known as North-South syndrome. North-South syndrome is a primary concern because of its potential to cause cerebral hypoxia, which has a critical influence on neurological complications often seen in this patient population. In order to reduce ischemic neurological complications, it is important to understand how clinical decisions regarding VA-ECMO parameters influence blood oxygenation. Here, we studied the impacts of flow rate and cannulation site on oxygenation using a one-dimensional (1D) model to simulate blood flow. Our model was initially tested by comparing blood flow results to those observed from experimental work in VA-ECMO patients. The 1D model was combined with a two-phase flow model to simulate oxygenation. Additionally, the influence of various other clinician-tunable parameters on oxygenation in the common carotid arteries (CCAs) were tested, including, blood viscosity, cannula position within the insertion artery, heart rate, and systemic vascular resistance (SVR), as well as geometrical changes such as arterial radius and length. Our results indicated that blood oxygenation to the brain strongly depended on the cannula insertion site and the VA-ECMO flow rate with a weaker but potentially significant dependence on arterial radius. During femoral cannulation, VA-ECMO flow rates greater than ~ 4.9 L/min were needed to perfuse the CCAs. However, axillary and central cannulation began to perfuse the CCAs at significantly lower flow (~ 1 L/min). These results may help explain the incidence of cerebral hypoxia in this patient population and the common need to change cannulation strategies during treatment to address this clinical problem. While this work describes patient-averaged results, determining these relationships between VA-ECMO parameters and cerebral hypoxia is an important step towards future work to develop patient-specific models that clinicians can use to improve outcomes.

☆ This manuscript has been authored by UT-Battelle, LLC under Contract No. DE-AC05-00OR22725 with the U.S. Department of Energy. The United States Government retains and the publisher, by accepting the article for publication, acknowledges that the United States Government retains a non-exclusive, paid-up, irrevocable, world-wide license to publish or reproduce the published form of this manuscript, or allow others to do so, for United States Government purposes. The Department of Energy will provide public access to these results of federally sponsored research in accordance with the DOE Public Access Plan(http://energy.gov/downloads/doe-public-access-plan).

* Corresponding author at: Department of Biomedical Engineering, Duke University, Durham, NC, USA.
E-mail address: amanda.randles@duke.edu (A. Randles).

https://doi.org/10.1016/j.jbiomech.2020.109707
0021-9290/

1. Introduction

Venoarterial extracorporeal membrane oxygenation (VA-ECMO) is a rapid support option for patients with cardiopulmonary failure and acts as a bridge to long term solutions such as native cardiac recovery, heart transplantation, or left ventricular assist devices. The number of cases and hospitals performing VA-ECMO has grown quickly in the past decade due to increased recognition of its benefits, access to equipment, and personnel training (ECLS, 2018). While this system is often vital for survival, ~15% of patients exhibit cerebral hypoxia that results from the VA-ECMO system (Squiers et al., 2016; Lorusso et al., 2016; Cheng et al., 2014). In fact, it is well-known that cerebral hypoxia is a major cause of impaired cognitive function in patients on cardiopulmonary bypass (Newman et al., 1994; Fearn et al., 2001). VA-ECMO is a complex system with many critical components that can be modified by a clinician, and a deeper understanding of how these clinician-tunable parameters impact blood oxygenation to the brain could help inform clinical decisions and improve neurological outcomes. During VA-ECMO patient support, deoxygenated blood is drained from the venous system, passed through an external pump and oxygenator, and returned to the body through a cannula typically placed in the femoral artery, such that native anterograde cardiac outflow pumps against retrograde VA-ECMO outflow, meeting in a region of the aorta known as the mixing zone. In patients with impaired pulmonary function, this process can result in North-South syndrome, where the upper body is perfused with poorly oxygenated cardiac outflow (Stevens et al., 2017; Makdisi and Wang, 2015; Zhong et al., 2016; Sorokin et al., 2017).

The femoral artery is the most common cannulation site because of its rapid implementation, but clinicians often move the insertion cannula to the axillary artery or aorta to reduce cerebral hypoxia. Aortic, or central, cannulation is the optimal choice for hemodynamics but requires a sternotomy or thoracotomy to directly access the aorta. Similarly, axillary cannulation requires a significant procedure in the operating room where a graft is sewn to the artery. In one study at Duke University, 60.7% of patients were cannulated in the femoral artery, 12.2% in the axillary artery, and 27.5% in the aorta. Clinicians generally choose the cannulation site based on arterial access, urgency of the procedure, and preexisting conditions (Ranney et al., 2017). With a more in depth understanding of how each cannulation site impacts hypoxia, clinicians can factor this crucial parameter into their decisions.

Measuring the impacts of various clinician-tunable parameters on oxygenation is difficult *in vivo*, and researchers are turning to computational fluid dynamics to simulate blood flow over wide ranges of parameters in a fast and cost-effective manner. To our knowledge, (Stevens et al., 2017, 2018) were the first group to use simulations showing that the mixing zone and blood oxygenation were highly influenced by VA-ECMO flow rates. The authors performed simulations across various flow rates in a three-dimensional (3D) geometry specifically for femorally cannulated patients. Similarly, (Gu et al., 2016, 2018) performed four VA-ECMO simulations with varying flow rates in an idealized 3D aorta and focused their studies on both flow to the brain and local hemodynamics such as wall shear stress. They found that volume of flow to the brain correlated with VA-ECMO flow rates, but they did not study any other input parameters and only considered central and femorally cannulated patients. Computational studies have also been performed comparing the effects of pulsatile and steady VA-ECMO flow (Zhang et al., 2018) in a single 3D model. The authors found that by carefully choosing the VA-ECMO pulse timing, they can achieve better upper limb perfusion.

The question still remains as to how various clinician-tunable parameters, such as cannulation site, VA-ECMO flow rate, cardiac output, blood viscosity, cannula position within the insertion artery, heart rate, and systemic vascular resistance (SVR), influence cerebral hypoxia. To investigate this open question, we developed a one-dimensional (1D) blood flow simulator (Boileau et al., 2015; Olufsen et al., 2000) coupled to a two-phase flow model to track oxygenation throughout the vasculature. With our 1D framework, we analyzed the influence of combinations of clinician-tunable parameters as well as geometrical parameters including artery diameter and length. Our results indicated that cannulation site and flow rate had the strongest influence on oxygenation with relatively little importance of other clinician-tunable parameters. Arterial length and diameter had small but potentially important impacts on oxygenation. We found that high VA-ECMO flow rates were necessary for adequate cerebral oxygenation with femoral cannulation, whereas significantly lower flow was needed with axillary and central cannulation. The patient-averaged model we built is a critical step towards a better understanding of the relationships between VA-ECMO parameters and cerebral hypoxia.

2. Methods

2.1. Vascular geometry

To accurately simulate blood flow in VA-ECMO patients, we needed to account for arterial flow behavior on the full body scale, with particular emphasis on vasculature reaching from the cannulation sites to the carotid arteries as well as the radial arteries which were used for model calibration (see Section 2.3). 1D models are a good choice to simulate blood flow over a large arterial geometry with fast run-times but make simplifying assumptions that may lead to less accurate results when compared with 3D models (Alastruey et al., 2012). The reduced computational load also enables large parameter sweeps and detailed sensitivity analyses that may not be feasible with 3D models (Diem and Bressloff, 2017; Boileau et al., 2015; Olufsen et al., 2000). Lumped parameter models are also a good choice for fast simulations. However, these models make further limiting assumptions and cannot be used to determine mixing zone locations, since they lose the axial spatial dimension (Shi et al., 2011).

Full body VA-ECMO scans are rarely taken in practice, so we used an adult male patient-averaged geometry developed by Sherwin et al. (2003), that describes the 55 largest arterial segments with lengths and radii in 1D. This model captures the regions of interest as well as many large distal arteries to account for downstream effects. Arteries were modeled as deformable tubes in a single axial dimension, and the insertion cannulae were modeled as rigid tubes inserted into either the femoral artery, axillary artery, or aortic root. Each artery had constant radius, a common assumption in 1D models (Wang, 2014; Sherwin et al., 2003). VA-ECMO draws blood from the venous system, but a model incorporating veins was not necessary since we focused on oxygenation in arteries. While studies have shown that the number of branches impacts flow rate and pressure, we fixed the total vessel number to focus exclusively on the impacts of VA-ECMO parameters (Vardhan et al., 2019; Giannopoulos et al., 2016). The number of vessels can be restricted in future work using data from patient-specific images. The full geometry is depicted in Fig. 1, and arterial properties are shown in Table 1.

2.2. VA-ECMO blood flow model development

The 1D blood flow simulator was developed in C++. The 1D governing equations describe the conservation of mass and momentum:

$$\frac{\partial A}{\partial t} + \frac{\partial Q}{\partial x} = 0 \tag{1}$$

Please cite this article as: B. Feiger, A. Kochar, J. Gounley et al., Determining the impacts of venoarterial extracorporeal membrane oxygenation on cerebral oxygenation using a one-dimensional blood flow simulator, Journal of Biomechanics, https://doi.org/10.1016/j.jbiomech.2020.109707

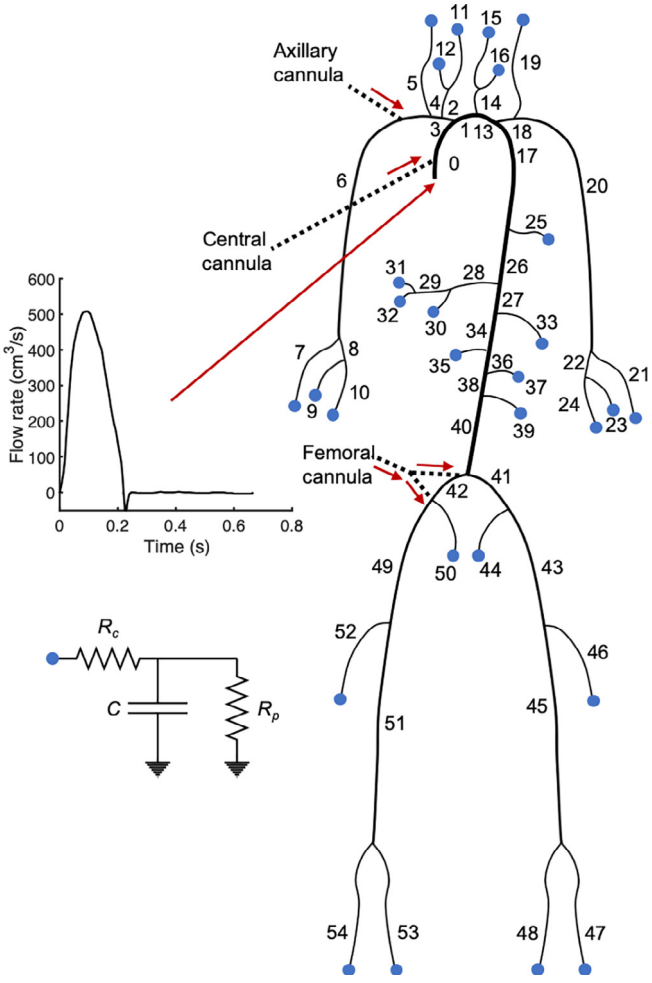

Fig. 1. The geometric model used in this study is based off of an adult male 1D model created by Sherwin et al. (2003). The model consists of the 55 largest arterial segments. Each arterial segment is numbered to correspond with its properties in Table 1. The inlets to the model were VA-ECMO cannulae located at either the axillary artery (axillary cannula), aorta (central cannula), or femoral artery (femoral cannula), as well as cardiac output. Each outlet, indicated with a blue circle, was coupled to a 3-element Windkessel boundary condition (Table 1). The red arrows indicate the direction of flow. The baseline waveform applied to the ascending aorta, derived from (Xiao et al., 2014), is also shown.

$$\frac{\partial Q}{\partial t}+\frac{\partial}{\partial x}\left(\alpha\frac{Q^2}{A}\right)+\frac{A}{\rho}\frac{\partial P}{\partial x}=-C_f\frac{Q}{A} \tag{2}$$

where A is the cross-sectional area, Q is the flow rate, P is the pressure, and $\rho = 1060\ \frac{\text{kg}}{\text{m}^3}$ is the density of blood. The term $C_f = 22\pi\nu$ represents friction that incorporates the dynamic viscosity $\nu = 4$ cP, and $\alpha = 1.1$ describes a somewhat flat velocity profile. The values used for α and C_f were adopted from experimental data and are commonly used in 1D blood flow models (Smith et al., 2002; Alastruey et al., 2011; Wang, 2014). The governing equations were solved with a MacCormack finite difference scheme.

To compute the location of the mixing zone and oxygen concentrations throughout the vasculature, a two-phase flow model was coupled to the 1D simulator. The purpose of the two-phase model was to track the volume fraction of VA-ECMO flow (VF_{ECMO}) versus left ventricular outflow (VF_{LV}). Distinguishing VA-ECMO flow from native cardiac output is important because each flow source has different blood oxygen concentrations. With knowledge of volume fractions and oxygen concentrations from each phase, we can compute total oxygen concentration at any location and timepoint throughout the vasculature. The two-phase flow model was based on the volume of fluid method that solves the 1D transport equation to advect volume fractions (Aniszewski et al., 2014):

$$\frac{\partial(VF_{ECMO})}{\partial t}+\left(\frac{Q}{A}\right)\frac{\partial(VF_{ECMO})}{\partial x}=0,\quad VF_{ECMO}+VF_{LV}=1. \tag{3}$$

Eq. (3) is implemented using a first order upwind scheme (Kajishima and Taira, 2017) at each time step after the flow field is computed from Eqs. (1) and (2) (Supplemental S1).

2.3. Inlet and outlet boundary conditions

To simulate VA-ECMO flow, the geometry required an inlet at the ascending aorta and another at various insertion cannula sites. A pulsatile inlet waveform at the ascending aorta was derived from (Xiao et al., 2014) (Fig. 1) and severely diminished to represent cardiac failure by scaling the waveform with constant factors such that the total flow rate (VA-ECMO flow and cardiac flow) was held constant at 5.5 L/min (Supplemental S3). As is typically seen clinically, we applied steady flow to the cannula inlet (Squiers et al., 2016). The heart rates and VA-ECMO flow rates used in this study were checked to ensure they were within the range of patient data obtained from the Duke University Medical Center under Institutional Review Board (IRB) approved protocols (Table 2). Data was gathered from adult VA-ECMO patients, and averages were used to guide inputs to the simulations. In each patient, the important parameters measured were VA-ECMO flow rate, heart rate, systolic pressure, and diastolic pressure.

A 3-element Windkessel lumped parameter model, consisting of two resistance values and one compliance value, was imposed at each outlet (Westerhof et al., 2009):

$$\left(1+\frac{R_c}{R_p}\right)Q+CR_c\frac{dQ}{dt}=\frac{P}{R_p}+C\frac{dP}{dt} \tag{4}$$

where R_c, R_p, and C are the characteristic resistance, peripheral resistance, and compliance, respectively. The 3-element Windkessel (Eqn 4) is a common choice to implement outlet boundary conditions by incorporating the effects of small distal arteries (Westerhof et al., 2009). Although a patient-averaged geometry was used in this study, we calibrated the model with patient data by tuning the resistances and compliances at the outlets to match patient pressures (Table 2). Specifically, the peripheral resistances and compliances were iterated until the resulting systolic and diastolic pressures were within 1% of the patient-averaged pressure data in the left radial artery (Supplemental figure S1). Iterations were performed manually with knowledge that increasing the compliance lowers the pulse pressure, and increasing the resistance raises the pressure. We were able to achieve convergence after ten manual iterations. The resulting 3-element Windkessel parameters are depicted in Table 1.

2.4. Study design

To ensure temporal convergence, all simulations were performed over 15 cardiac cycles, and the last cycle was used for analysis.

2.4.1. Assessing the accuracy and validity of the model

Demonstrating that the 1D simulator is capable of modeling VA-ECMO flow required model verification as well as testing against VA-ECMO patient data. We verified our simulator by comparing the simulation results to analytical solutions in a pipe and bifurcation geometry. Additionally, we tested our simulator by comparing simulation results with computational studies performed by Xiao et al. (2014) to show how our simulator performs in a larger geometry. We chose to use the most complex geometry

Please cite this article as: B. Feiger, A. Kochar, J. Gounley et al., Determining the impacts of venoarterial extracorporeal membrane oxygenation on cerebral oxygenation using a one-dimensional blood flow simulator, Journal of Biomechanics, https://doi.org/10.1016/j.jbiomech.2020.109707

Table 1
The 1D geometry and the Windkessel parameters are described in this table.

ID	Artery	Length (cm)	Radius (cm)	β (g s^{-2} cm^{-2})	R_p (g s^{-1} cm^{-4})	R_c (g s^{-1} cm^{-4})	C (cm^4 s^2 g^{-1})
0	Ascending Aorta	4	1.38	9.70E+04			
1	Aortic Arch I	2	1.28	8.70E+04			
2	Brachiocephalic	3.4	0.62	2.33E+05			
3	Right Subclavian I	3.4	0.42	4.23E+05			
4	Right Carotid	17.7	0.37	5.16E+05			
5	Right Vertebral	14.8	0.2	2.59E+06	7.17E+04	1.81E+04	1.72E−06
6	Right Subclavian II	42.2	0.4	4.66E+05			
7	Right Radial	23.5	0.19	2.87E+06	4.57E+04	1.15E+04	2.70E−06
8	Right Ulnar I	6.7	0.22	2.25E+06			
9	Right Interosseous	7.9	0.1	1.29E+07	1.89E+05	4.78E+04	6.52E−07
10	Right Ulnar II	17.1	0.2	2.45E+06	4.65E+04	1.17E+04	2.65E−06
11	Right Internal Carotid	17.6	0.2	2.64E+06	2.28E+04	5.76E+03	5.41E−06
12	Right External Carotid	17.7	0.2	2.47E+06	3.72E+04	9.39E+03	3.32E−06
13	Aortic Arch II	3.9	1	1.30E+05			
14	Left Carotid	20.8	0.37	5.19E+05			
15	Left Internal Carotid	17.6	0.2	2.64E+06	2.29E+04	5.78E+03	5.39E−06
16	Left External Carotid	17.7	0.2	2.47E+06	3.73E+04	9.42E+03	3.31E−06
17	Thoracic Aorta I	5.2	1	1.24E+05			
18	Left Subclavian I	3.4	0.42	4.16E+05			
19	Vertebral	14.8	0.2	2.59E+06	7.62E+04	1.92E+04	1.62E−06
20	Left Subclavian II	42.2	0.4	4.66E+05			
21	Left Radial	23.5	0.19	2.87E+06	4.49E+04	1.13E+04	2.75E−06
22	Left Ulnar I	6.7	0.22	2.24E+06			
23	Left Interosseous	7.9	0.1	1.29E+07	1.90E+05	4.80E+04	6.49E−07
24	Left Ulnar II	17.1	0.2	2.45E+06	4.74E+04	1.20E+04	2.60E−06
25	Intercostals	8	0.25	8.85E+05	3.96E+04	8.00E+03	1.65E−06
26	Thoracic Aorta II	10.4	0.98	1.17E+05			
27	Abdominal I	5.3	0.78	1.67E+05			
28	Celiac I	2	0.39	4.75E+05			
29	Celiac II	1	0.2	1.81E+06			
30	Hepatic	6.6	0.22	1.14E+06	1.33E+04	3.35E+03	9.31E−06
31	Gastric	7.1	0.18	1.57E+06	1.36E+06	3.43E+05	9.08E−08
32	Splenic	6.3	0.28	8.06E+05	1.87E+04	4.73E+03	6.58E−06
33	Superior Mesenteric	5.9	0.37	5.69E+05	8.64E+03	2.18E+03	1.43E−05
34	Abdominal II	1	0.63	2.27E+05			
35	Left Renal	3.2	0.32	5.66E+05	8.96E+03	2.26E+03	1.38E−05
36	Abdominal III	1	0.57	2.78E+05			
37	Right Renal	3.2	0.23	1.18E+06	8.99E+03	2.27E+03	1.37E−05
38	Abdominal IV	10.6	0.47	3.81E+05			
39	Inferior Mesenteric	5	0.16	1.90E+06	9.47E+04	2.39E+04	1.30E−06
40	Abdominal V	1	0.43	3.99E+05			
41	Right Common Iliac	5.9	0.32	6.49E+05			
42	Left Common Iliac	5.8	0.32	6.49E+05			
43	Left External Iliac	14.4	0.28	1.49E+06			
44	Left Internal Iliac	5	0.24	3.13E+06	1.65E+04	4.16E+03	7.49E−06
45	Left Femoral	44.3	0.21	2.56E+06			
46	Left Deep Femoral	12.6	0.2	2.65E+06	1.36E+04	3.43E+03	9.09E−06
47	Left Posterior Tibial	32.1	0.19	5.81E+06	8.38E+04	2.12E+04	1.47E−06
48	Left Anterior Tibial	34.3	0.14	9.24E+06	9.71E+04	2.45E+04	1.27E−06
49	Right External Iliac	14.5	0.28	1.49E+06			
50	Right Internal Iliac	5.1	0.24	3.13E+06	1.64E+04	4.15E+03	7.51E−06
51	Right Femoral	44.4	0.21	2.56E+06			
52	Right Deep Femoral	12.7	0.2	2.65E+06	1.36E+04	3.43E+03	9.09E−06
53	Left Posterior Tibial	32.2	0.19	5.81E+06	8.38E+04	2.12E+04	1.47E−06
54	Right Anterior Tibial	34.4	0.14	9.24E+06	9.71E+04	2.45E+04	1.27E−06

Table 2
Patient data shown as mean and standard deviation (n = 5).

Patient Parameters	Patient Averaged Data
Age	57 ± 15.1
Height (cm)	166.2 ± 3.5
Weight (kg)	86.3 ± 7.8
Heart rate (beats/min)	91.0 ± 11.5
Systolic pressure (mmHg)	91.7 ± 22.8
Diastolic pressure (mmHg)	83.0 ± 23.9
ECMO flow rate (L/min)	4.5 ± 0.4

in their work for comparisons, which included vasculature extending from the ascending aorta to the iliac arteries (Fig. 2, Table 3).

Finally, we tested the ability of our simulator to model VA-ECMO flow by comparing simulation results to VA-ECMO patient data from (Cevasco et al., 2018) showing how mean pulsatility indices (MPIs) varied based on insertion cannula site. MPIs were computed as follows (Eq. (5)):

$$\mathrm{MPI} = \frac{\text{systolic pressure} - \text{diastolic pressure}}{\text{mean pressure}} \tag{5}$$

We used the full body geometry for this analysis (Fig. 1). Because we lacked patient-specific data, we sought to ensure that the general trends seen in the simulations and literature were similar rather than precisely matching literature values. Cevasco et al. (2018) computed MPI in the middle cerebral arteries, whereas we computed MPI in the internal carotid arteries (ICAs) as those arteries feed into the middle cerebral arteries. We chose to compute MPI values as ratios to the maximum MPI (MPI ratio), which occurred in the right ICAs with femoral cannulation in our simulation results

Please cite this article as: B. Feiger, A. Kochar, J. Gounley et al., Determining the impacts of venoarterial extracorporeal membrane oxygenation on cerebral oxygenation using a one-dimensional blood flow simulator, Journal of Biomechanics, https://doi.org/10.1016/j.jbiomech.2020.109707

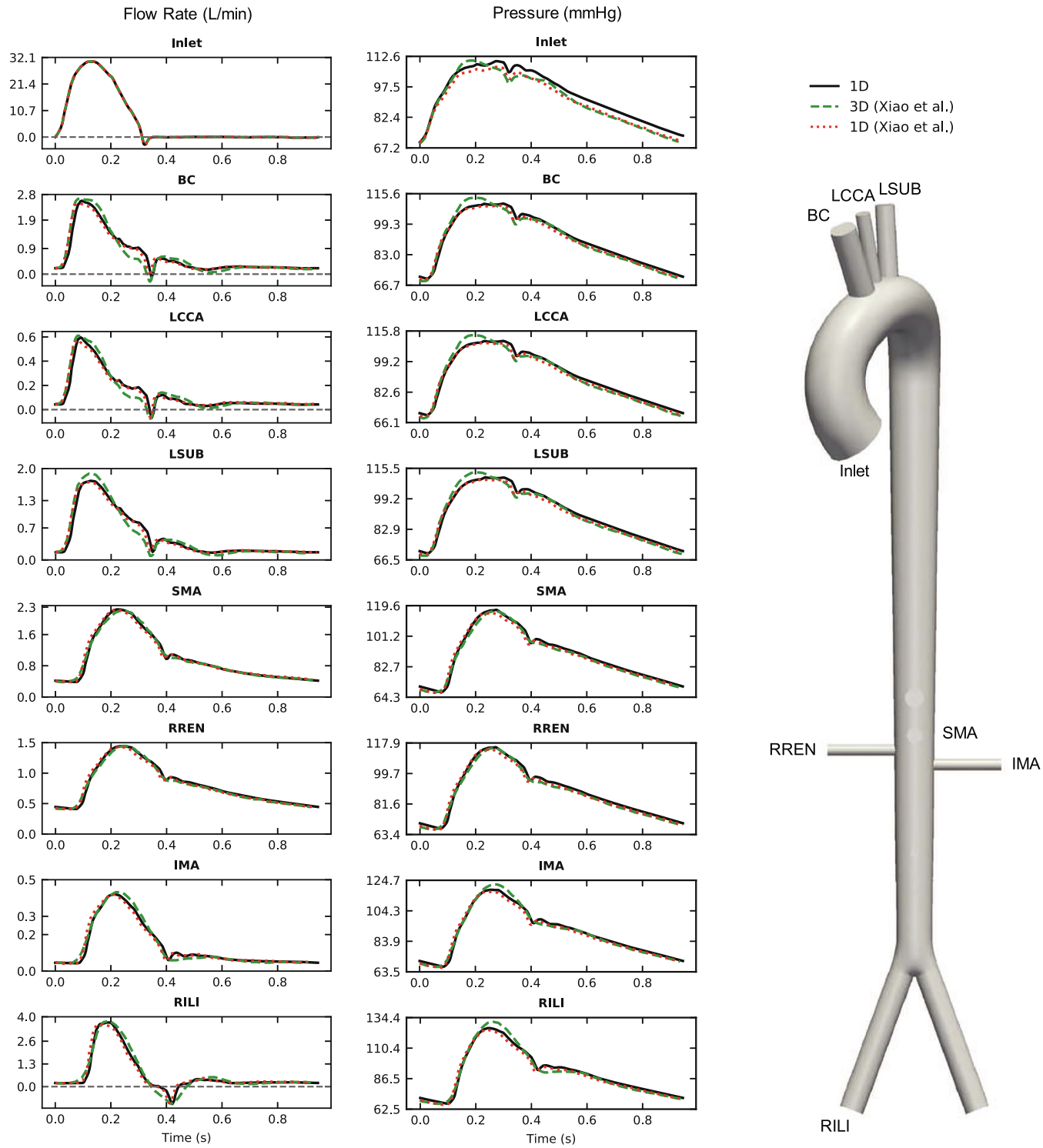

Fig. 2. Comparison of the 1D simulator with 1D and 3D computations performed by Xiao et al. (2014). The geometry is shown on the right, which consists of ten aortic segments and nine branches. Flow rates and pressures were compared at the inlet of the ascending aorta and the outlets of seven arteries - brachiocephalic artery (BC), left common carotid artery (LCCA), left subclavian artery (LSUB), superior mesenteric artery (SMA), right renal artery (RREN), inferior mesenteric artery (IMA), and right iliac artery (RILI).

and the right middle cerebral artery in the experimental work, to give a more general metric that could potentially scale similarly in different geometries. To ensure the MPI ratio results were not highly sensitive to input parameters, we swept over three parameters that were likely to influence pulsatility: vessel stiffness (β), total arterial compliance, and peripheral resistance (Further details on model verification and testing with patient data can be found in Supplemental S2).

2.4.2. Sensitivity analyses for blood oxygenation

Sensitivity analyses were performed to determine which parameters had the strongest influence on mixing zone location

Please cite this article as: B. Feiger, A. Kochar, J. Gounley et al., Determining the impacts of venoarterial extracorporeal membrane oxygenation on cerebral oxygenation using a one-dimensional blood flow simulator, Journal of Biomechanics, https://doi.org/10.1016/j.jbiomech.2020.109707

Table 3
A geometry from (Xiao et al., 2014) was used to test the 1D blood flow simulator. Several of the arteries from their work were tapered and had varying β values along the length of the artery. In our model, we used the vessel average diameter and β value.

Artery	Length (cm)	Radius - Xiao et al. (cm)	Radius (cm)	β - Xiao et al. ($g\ s^{-2}\ cm^{-2}$)	β ($g\ s^{-2}\ cm^{-2}$)	R_p ($g\ s^{-1}\ cm^{-4}$)	R_c ($g\ s^{-1}\ cm^{-4}$)	C ($cm^4\ s^2\ g^{-1}$)
Ao I	7.0357	1.52 → 1.39	1.455	1.79E+05 → 2.07E+05	1.93E+05			
Ao II	0.8	1.39 → 1.37	1.38	2.07E+05 → 2.12E+05	2.10E+05			
Ao III	0.9	1.37 → 1.35	1.36	2.12E+05 → 2.16E+05	2.14E+05			
Ao IV	6.4737	1.35 → 1.23	1.29	2.16E+05 → 2.52E+05	2.33E+05			
Ao V	15.2	1.23 → 0.99	1.11	2.52E+05 → 3.56E+05	2.98E+05			
Ao VI	1.8	0.99 → 0.97	0.98	3.56E+05 → 3.68E+05	3.62E+05			
Ao VII	0.7	0.97 → 0.962	0.966	3.68E+05 → 3.73E+05	3.70E+05			
Ao VIII	0.7	0.962 → 0.955	0.9585	3.73E+05 → 3.77E+05	3.75E+05			
Ao IX	4.3	0.955 → 0.907	0.931	3.77E+05 → 4.09E+05	3.93E+05			
Ao X	4.3	0.907 → 0.86	0.8835	4.09E+05 → 4.46E+05	4.27E+05			
Brachiocephalic	3.4	0.635 → 0.635	0.635	7.24E+05 → 7.24E+05	7.24E+05	1.06E+04	5.19E+02	8.70E−05
L. com carotid	3.4	0.36 → 0.36	0.36	1.80E+06 → 1.80E+06	1.80E+06	5.22E+04	1.92E+03	1.77E−05
L. subclavian	3.4	0.48 → 0.48	0.48	1.14E+06 → 1.14E+06	1.14E+06	1.30E+04	9.88E+02	7.09E−05
Celiac	3.2	0.445 → 0.445	0.445	1.28E+06 → 1.28E+06	1.28E+06	7.57E+03	1.18E+03	1.22E−04
Sup. mesenteric	6	0.375 → 0.375	0.375	1.69E+06 → 1.69E+06	1.69E+06	5.51E+03	1.74E+03	1.67E−04
R. renal	3.2	0.28 → 0.28	0.28	2.69E+06 → 2.69E+06	2.69E+06	5.39E+03	3.41E+03	1.71E−04
L. renal	3.2	0.28 → 0.28	0.28	2.69E+06 → 2.69E+06	2.69E+06	5.39E+03	3.41E+03	1.71E−04
Inf. mesenteric	5	0.2 → 0.2	0.2	4.60E+06 → 4.60E+06	4.60E+06	4.62E+04	7.40E+03	2.00E−05
R. com. iliac	8.5	0.6 → 0.6	0.6	7.94E+05 → 7.94E+05	7.94E+05	1.02E+04	5.91E+02	9.07E−05
L. com. iliac	8.5	0.6 → 0.6	0.6	7.94E+05 → 7.94E+05	7.94E+05	1.02E+04	5.91E+02	9.07E−05

Table 4
Parameters are shown as the baseline values ± the range used for analyses. VA-ECMO flow rate did not have a baseline value since every study conducted in this work varied that parameter. Femoral cannula position refers to the cannula location within the vessel itself, not across cannula insertion sites.

Parameter	Range
ECMO flow rate (L/min)	1–5.5
Viscosity (cP)	4 ± 1
Peripheral resistance scale factor	1 ± 0.5
Cardiac cycle time (s)	0.7 ± 0.15
Femoral cannula position	Along length of iliac artery
Cannula insertion site	Femoral artery, axillary artery, or aorta

and blood oxygenation in the left common carotid artery (LCCA) in femorally cannulated patients. We focused this component on clinician-tunable parameters, including VA-ECMO flow rate, heart rate, SVR, blood viscosity, and VA-ECMO insertion cannula position (Supplemental S3) (Table 4). Sensitivity analyses were performed using the Sobol method implemented in the open source Python library SALib (Sobol et al., 2007; Eck et al., 2016) and tested the influence of individual as well as combinations of parameters. The first-order sensitivity index (S_i) is given by the following equation (Eqn 6):

$$S_i = \frac{V[E[Y \mid Z_i]]}{V[Y]} \tag{6}$$

where S_i represents the amount that input parameter Z_i contributes to the total variance of the output parameter $V[Y]$. $E[Y \mid Z_i]$ represents the expected value of the output parameter Y given a fixed input parameter Z_i. Higher order sensitivity indices can be computed to determine the influence of combinations of input parameters on output variables. Here, we compute total sensitivity indices, which represent the direct effect of an individual input parameter as well as its interactions with all other inputs. The total sensitivity index $S_{T,i}$ is computed as follows (Eqn 7):

$$S_{T,i} = 1 - \frac{V[E[Y \mid Z_{-i}]]}{V[Y]} \tag{7}$$

where Z_{-i} represents all the inputs excluding Z_i. We used the Saltelli method to uniformly generate 10,000 combinations of input parameters, which we deemed sufficient to fully understand the contribution of each input parameter.

To determine the location of the mixing zone, we started from the ascending aorta and traveled down the aorta until the proportion of VA-ECMO flow reached at least 0.5 ($VF_{ECMO} \geqslant 0.5$) at any time point during the cardiac cycle. The distance from the mixing zone location to the insertion cannula was recorded.

2.4.3. Determining the influence of VA-ECMO flow rate on oxygenation

To further probe the influence of VA-ECMO flow rate, we swept across 1,000 flow rate values, while holding all other clinician-tunable parameters constant. We assumed that 1,000 values were enough to fully delineate the flow rate parameter space. Additionally, we chose to vary two geometrical parameters - arterial diameter and length - to determine how they influence oxygenation results. While arterial anatomies in VA-ECMO patients will likely have a wide variation, such as location and spacing of arteries, we focused this study on diameter and length due to the difficulty in acquiring VA-ECMO patient-specific images. The diameters were held at baseline, reduced by 10%, or raised by 20%, following the work of (Willemet et al., 2015), and the arterial lengths were held at baseline or raised/lowered by 20% (Smulyan et al., 1998). Simulations varying the arterial length and diameter were held at baseline diameter and baseline length values, respectively. For simulations with femoral cannulation, the location of the mixing zone and the VF_{ECMO} in the common carotid arteries (CCAs) were computed. For central and axillary cannulation, only the VF_{ECMO} in the CCAs was computed as these cannulation sites are not known to produce a mixing zone.

3. Results

3.1. 1D simulator verification, calibration, and testing

All simulations performed in this work are listed in Table 5. We performed verification, calibration, and testing of our model for blood flow in VA-ECMO patients. Verification was tested with flow in a pipe, where flow rate was plotted against distance along the pipe for a half sine wave input, showing good agreement between the analytical and simulated solution (Supplemental figure S2a and S2b). We also verified flow through a bifurcation with the same inlet condition and computed the reflected and transmitted waves. Once again, we saw good agreement between the simulated and analytical results (Supplemental figure S2c).

Please cite this article as: B. Feiger, A. Kochar, J. Gounley et al., Determining the impacts of venoarterial extracorporeal membrane oxygenation on cerebral oxygenation using a one-dimensional blood flow simulator, Journal of Biomechanics, https://doi.org/10.1016/j.jbiomech.2020.109707

Table 5
Each simulation performed in this worked is listed along with the purpose of the simulation and the figure or table showing the results.

Simulation	Goal	Results Figure/ Table
	Model verification, calibration, and testing	
Simulator verification	Comparing our 1D simulator to an analytical solution	Figure S2
Simulator calibration	Tuning the boundary conditions to match VA-ECMO patient data from the Duke University Medical Center	Figure S1
Testing simulator against other work	Comparing our 1D simulator to a well-known simulator from Xiao et al. (2014)	Fig. 2
Testing Simulator against VA-ECMO data	Testing model against VA-ECMO patient data from literature	Table S1
Sensitivity analysis for testing with VA-ECMO patient data	Determine how sensitive the results are to input parameters when comparing simulations with VA-ECMO patient data from literature	Figure S3
	Sensitivity analysis	
Sensitivity analysis	Determine which physician-tunable parameters contribute to oxygenation and mixing zone location	Table 6
	Mixing zone and oxygenation studies	
Mixing zone location	Determine how changes in flow rate impact the location of the mixing zone	Fig. 3
Carotid oxygenation	Determine how changes in flow rate as well as changes in arterial diameter and length impact oxygenation in the CCAs	Figs. 4 and 5

To test the model on VA-ECMO patient data from literature, MPI ratios in the ICAs for femoral, axillary, and central cannula insertion locations were computed and compared to work from (Cevasco et al., 2018). Results show that MPI ratios were similar between simulations and literature (Supplemental table S1). In each cannulation location, the left ICA had a smaller MPI than the right side. Additionally, femoral cannulation resulted in the highest MPI followed by central cannulation, and axillary cannulation had the smallest. To ensure our results were not highly subject to model assumptions, we performed sensitivity analyses with three parameters that are likely to impact blood flow pulsatility: artery stiffness, peripheral vascular resistance, and total arterial compliance. Results showed that total arterial compliance and peripheral resistance had almost no impact on MPI ratio. Vessel stiffness had a larger impact where MPI ratios changed by nearly 20% in the right ICA (Supplemental figure S3).

We also compared our 1D simulator with computational work performed by Xiao et al. (2014). Pressure and flow rate comparisons were shown for six different arteries in the model. Our 1D results were similar to the 1D and 3D results found by the authors, with some minor differences across each artery. The inlet pressure had the most extensive difference between our 1D results and the authors' work. This is likely due to the authors using tapered vessels whereas we used vessels with constant diameter. However, the values were still within 5% in the worst case scenario (Fig. 2).

3.2. Influence of clinician-tunable VA-ECMO parameters on blood oxygenation

To identify the influence of each parameter, we performed sensitivity analyses that indicated which clinician-tunable parameters most strongly influenced mixing zone location and blood oxygenation for femoral cannulation. Results showed that the VA-ECMO flow rate had the largest influence on both mixing zone location and blood oxygenation with minimal influence from viscosity, peripheral resistance, heart rate, and cannula position (Table 5). We note that these sensitivity analyses do not account for various cannula insertion sites.

3.3. Influence of VA-ECMO flow rate on blood oxygenation

Based on the results of the sensitivity analyses, we studied how VA-ECMO flow rate altered the mixing zone location while holding all other clinician-tunable parameters at their respective baseline values. VA-ECMO flow rate was plotted against distance from the insertion cannula location, demonstrating how the mixing zone location migrates proximally towards the left ventricle as VA-ECMO flow rate increases (Fig. 3).

Finally, we assessed oxygenation in the LCCA and right CCA (RCCA) by computing VF_{ECMO} with femoral, axillary, and central cannulation. All three cannulation strategies were included in this study because each strategy has a potentially different impact on blood oxygenation in the brain. VA-ECMO flow rate was plotted against VF_{ECMO} for each cannulation site, showing significantly different VF_{ECMO} in the LCCA and RCCA for all three cannulation strategies (Figs. 4 and 5). Briefly, femoral cannulation required high flow rates before VA-ECMO flow reached the CCAs, whereas axillary and central cannulation began to oxygenate the CCAs at low flow rates. Arterial diameter had minor impacts during femoral cannulation but larger effects with axillary and central cannulation, where larger diameter arteries tended to result in higher oxygen concentration in the CCAs (Fig. 4). Arterial length demonstrated a similar trend where longer arteries led to higher CCA oxygenation, particularly with central cannulation (Fig. 5).

4. Discussion

VA-ECMO support is often vital for patient survival, but it is frequently associated with neurological complications resulting from cerebral hypoxia (Lorusso et al., 2016). In fact, significant resources

Table 6
The sensitivities of the mixing zone location and oxygenation in the LCCA were computed for various parameters shown in the table. S1 refers to the first order sensitivity index, and ST refers to the total sensitivity index. Sensitivity indices closer to one indicate a higher contribution to the variance in the mixing zone location. Cannula position refers to the location of the cannula within the femoral artery.

Sensitivity Target	Sensitivity Index	VA-ECMO Flow Rate	Viscosity	Peripheral Resistance	Heart Rate	Cannula Position
Mixing zone location	S1	0.96	0.002	−0.003	−0.002	0.001
	ST	1	0.003	0.022	0.016	0.006
LCCA oxygenation	S1	1.01	0.001	0	0.002	0
	ST	1.01	0	0.001	0.002	0

Please cite this article as: B. Feiger, A. Kochar, J. Gounley et al., Determining the impacts of venoarterial extracorporeal membrane oxygenation on cerebral oxygenation using a one-dimensional blood flow simulator, Journal of Biomechanics, https://doi.org/10.1016/j.jbiomech.2020.109707

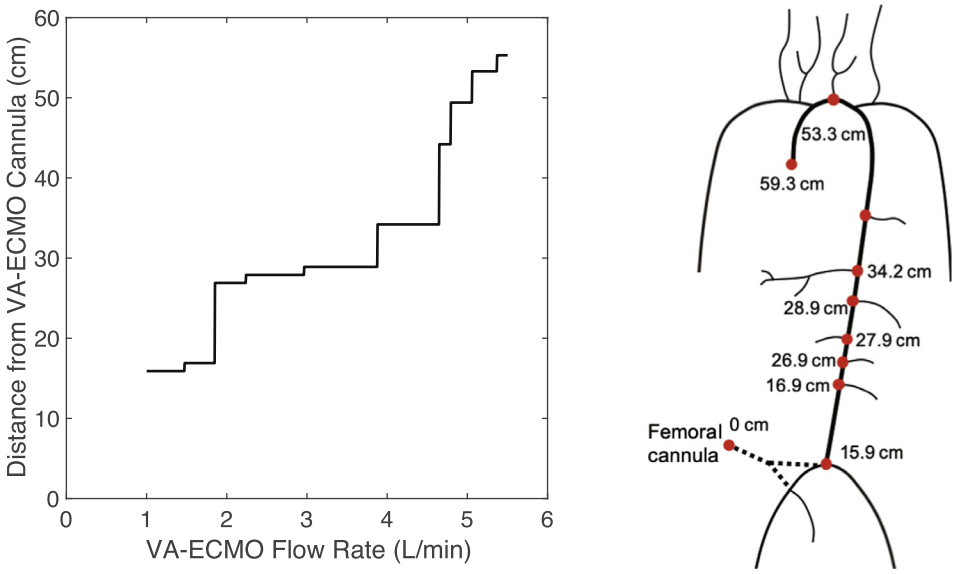

Fig. 3. The location of the mixing zone within the aorta was computed at 1,000 different VA-ECMO flow rates for a femorally cannulated patient. The plot shows the location of the mixing zone as a function of VA-ECMO flow rate. The 1D image on the right shows some sample distance measurements between the femoral cannula and aortic root. The location is recorded as a distance from the insertion cannula. The geometry was cut off in the image for illustration purposes.

are often spent monitoring brain oxygenation in this patient population (Le Guennec et al., 2018; Kazmi et al., 2018; Kim et al., 2019). While simulations are unlikely to replace physical monitoring techniques, they can be used to predict and better understand how clinicians' choices impact cerebral hypoxia. To model hemodynamics, we developed a 1D simulator capable of modeling various combinations of clinician-tunable parameters. From our sensitivity analyses, we hypothesized that flow rate was the most influential parameter. However, the effects of other clinician-tunable parameters on oxygenation remained unclear. The minimal contribution by each clinician-tunable parameter other than flow rate was an interesting result and allowed us to focus the remainder of the study on flow rate. While simulating the influence of VA-ECMO flow rates on oxygenation, we varied the cannulation site between femoral, axillary, and central, and also varied arterial diameter and length.

To oxygenate the CCAs with femoral cannulation, a higher flow rate was needed compared with axillary or central cannulation due to the increased distance between the CCAs and the insertion cannula. While this result could be predicted based on the increased distance from the femoral cannula to the left ventricle, the flow rates needed to oxygenate the brain from each cannula location were unknown. Oxygenated blood began to reach the LCCA and RCCA at flow rates of ~ 5 L/min and ~ 5.3 L/min, respectively. In the RCCA, the VF_{ECMO} only reached ~ 0.3 even at the highest flow rates, which indicates that providing adequate amounts of oxygenated blood to the RCCA with femoral cannulation could be challenging. These results are similar to those observed by Stevens et al. (2017) who showed that the brachiocephalic arteries were mostly perfused with cardiac flow even when VA-ECMO flows consisted of 85% of the total flow. They additionally demonstrated that VA-ECMO flows consisting of 75% of the total flow were needed to perfuse the LCCA, further agreeing with our results. Often, femorally cannulated patients require clinicians to change the cannula location or add an additional cannula due to poor oxygenation. For example, work by Pavlushkov et al. (2017) describes patients with poor upper body oxygenation that need extensive changes to their treatment plans such as adjusting ventilator settings, using diuretics, or adding another cannula to insert oxygenated blood closer to the heart. None of these options are ideal for patients who are already in critical condition. Our results provide a step in the right direction towards reducing the need for these changes by better predicting oxygenation. Unlike femoral cannulation, axillary and central cannulation results showed that the RCCA was well perfused with VA-ECMO flow at low flow rates.

Our study on mixing zone location (Fig. 3) indicates a reason for the reduced oxygenation in the CCAs with femoral cannulation as the mixing zone location was typically located between the renal arteries and the ascending aorta except for very low VA-ECMO flow rates. This is consistent with reports by Napp et al. (2016) who saw similar observations for patients in clinical settings. Napp et al. (2016) also mention that the brachiocephalic artery and LCCA were perfused via the heart in most patients. While it was not surprising that the mixing zone migrated proximally towards the heart with increased VA-ECMO flow rates, the velocity and locations of migration were unknown. Ideally, clinicians would continue to increase VA-ECMO flow rates in a clinical setting to ensure adequate oxygenation to the cerebral vasculature. However, raising the flow rate to large values can result in high shear from the centrifugal pump and increased afterload on the left ventricle (Sakota et al., 2008; Meani and Pappalardo, 2017).

Finally, we tested the impacts of arterial diameter and length on CCA oxygenation. While these parameters are unlikely to be measured in VA-ECMO patients, they provide an interesting biomechanics study indicating how simple geometrical changes influence oxygenation. Evidence suggests that several diseases such as obesity and impaired glucose tolerance are associated with larger arterial diameters (van Dijk et al., 2000; Wildman et al., 2004) which could influence flow. Arterial length is strongly correlated with patient height and is therefore, an important parameter to study (Smulyan et al., 1998). However, few studies, have investigated the relationship between patient height and neurological outcomes in VA-ECMO patients. Our results showed that axillary and central cannulated patients with larger arterial diameters exhibit higher oxygen concentrations in the CCAs. Additionally, arterial length had a potentially significant impact with central cannulation where longer arteries led to higher oxygenation in the CCAs. As the VA-ECMO flow rates grew, differences in oxygenation based on length tended to grow smaller (Fig. 4).

Please cite this article as: B. Feiger, A. Kochar, J. Gounley et al., Determining the impacts of venoarterial extracorporeal membrane oxygenation on cerebral oxygenation using a one-dimensional blood flow simulator, Journal of Biomechanics, https://doi.org/10.1016/j.jbiomech.2020.109707

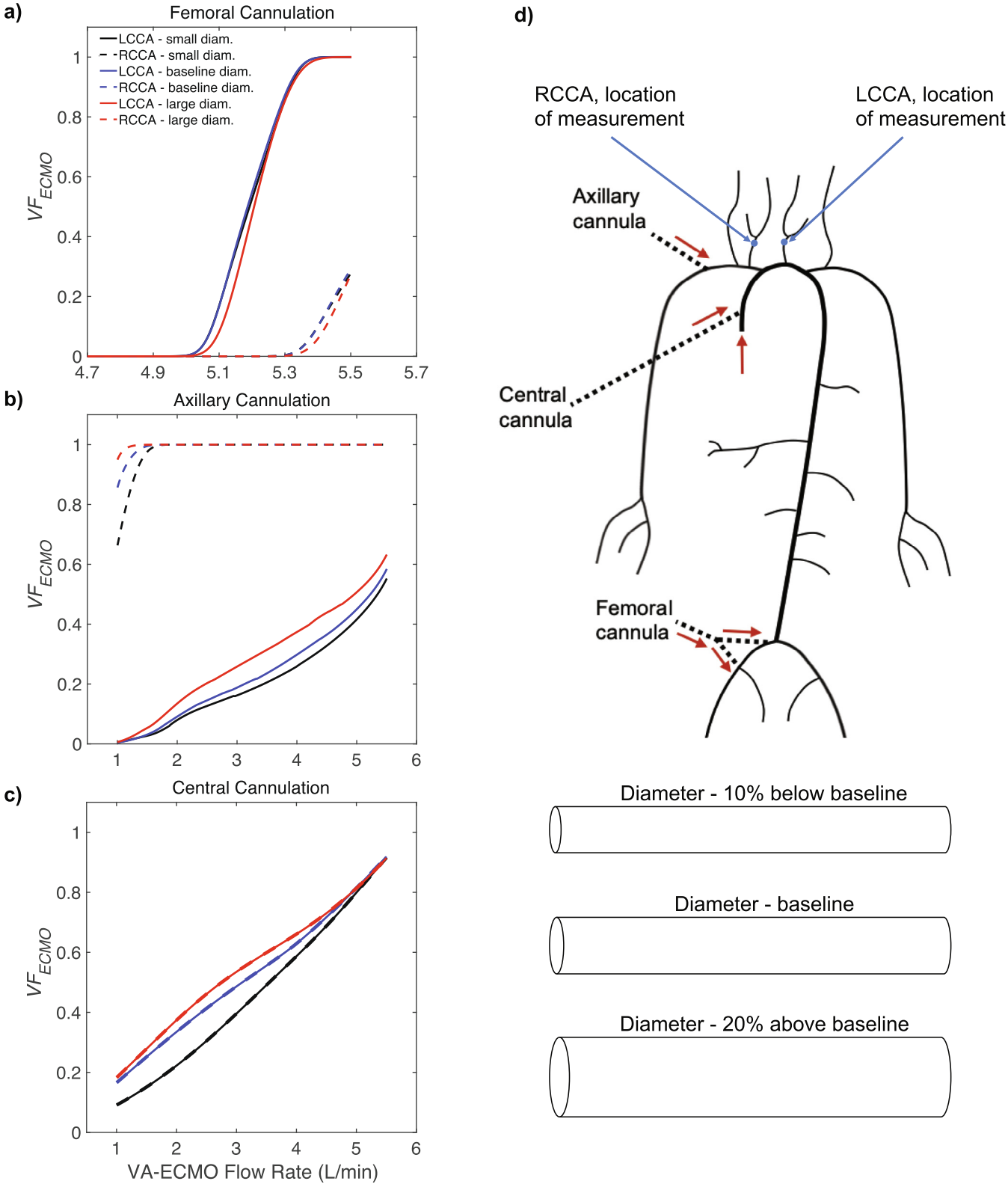

Fig. 4. The VF_{ECMO} was computed at the ends of the left common carotid artery (LCCA) and right common carotid artery (RCCA) as a function of VA-ECMO flow rate for various changes in arterial diameter. Each artery was altered from its baseline diameter by either reducing the diameter by 10% (small diam) or increasing the diameter by 20% (large diam). Simulations were performed for (a) femoral cannulation, (b) axillary cannulation, and (c) central cannulation. (d) Depicts the cannulation sites with blue arrows pointing to the measurement locations in the LCCA and RCCA and depicts the arterial diameter changes. The geometry was cut off in the image for illustration purposes.

Please cite this article as: B. Feiger, A. Kochar, J. Gounley et al., Determining the impacts of venoarterial extracorporeal membrane oxygenation on cerebral oxygenation using a one-dimensional blood flow simulator, Journal of Biomechanics, https://doi.org/10.1016/j.jbiomech.2020.109707

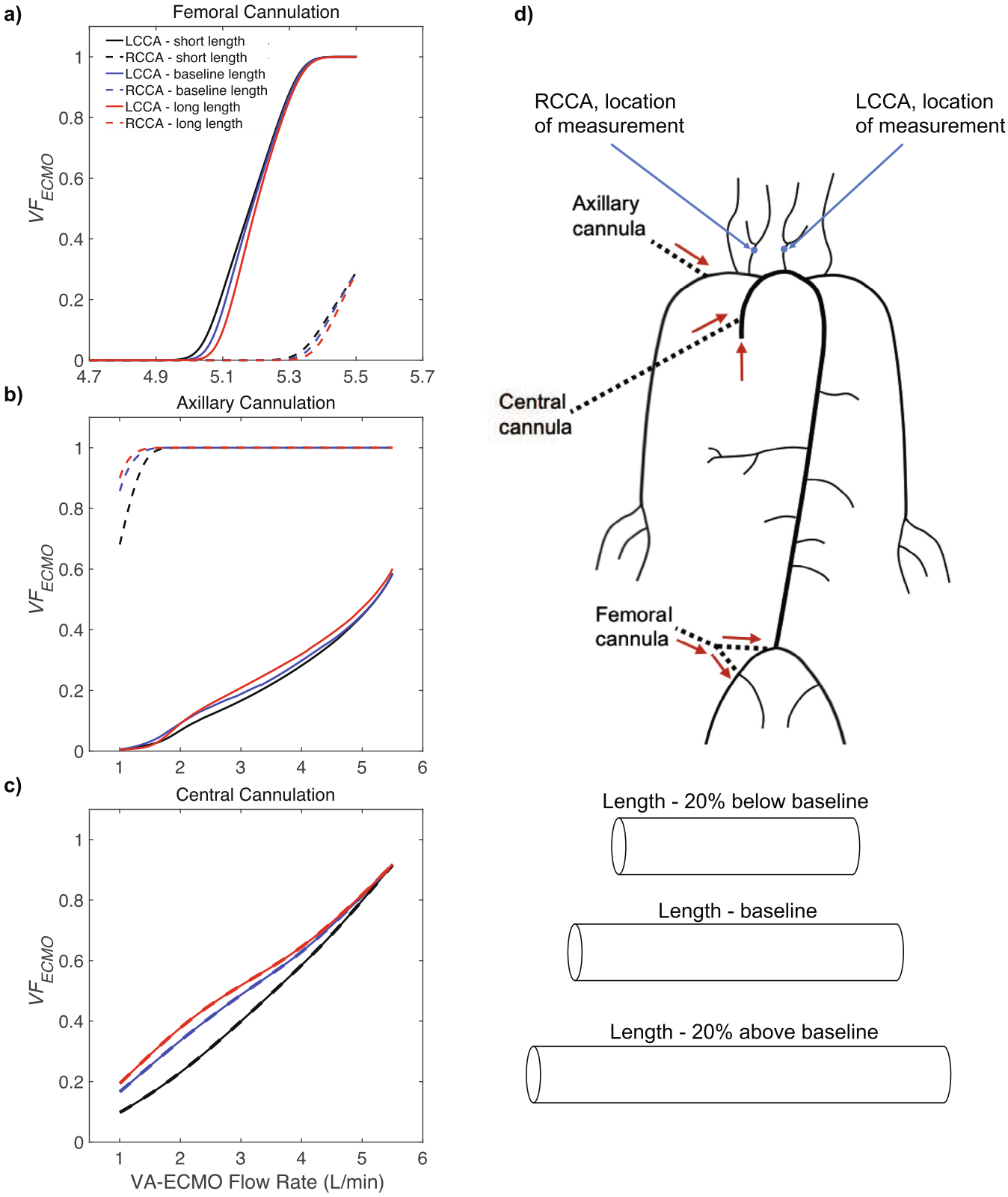

Fig. 5. The VF_{ECMO} was computed at the ends of the left common carotid artery (LCCA) and right common carotid artery (RCCA) as a function of VA-ECMO flow rate for various changes in arterial length. Each artery was altered from its baseline length by either reducing the length by 20% (short length) or increasing the length by 20% (long length). Simulations were performed for (a) femoral cannulation, (b) axillary cannulation, and (c) central cannulation. (d) Depicts the cannulation sites with blue arrows pointing to the measurement locations in the LCCA and RCCA and depicts the arterial length changes. The geometry was cut off in the image for illustration purposes.

Please cite this article as: B. Feiger, A. Kochar, J. Gounley et al., Determining the impacts of venoarterial extracorporeal membrane oxygenation on cerebral oxygenation using a one-dimensional blood flow simulator, Journal of Biomechanics, https://doi.org/10.1016/j.jbiomech.2020.109707

4.1. Limitations

One of the limitations of our work is the lack of patient-specific parameters. While supporting a patient with VA-ECMO, it is often difficult to obtain patient-specific scans and cardiac outflow rates due to mechanical and equipment constraints, cost, and patient safety. While we varied arterial diameters and radii, we did not change network connectivity, which includes the position of arteries with respect to each other, and the total vessel number. The total vessel number has been shown to impact flow rate, pressure, and local hemodynamic parameters in arterial networks (Vardhan et al., 2019; Giannopoulos et al., 2016). Limiting the simulations to one patient-averaged geometry allowed us to focus on the influence of clinician-tunable parameters. Holding the geometry constant is consistent with other VA-ECMO simulation studies (Stevens et al., 2018, 2017; Gu et al., 2018, 2016; Zhang et al., 2018). Another limitation is the assumption that the diameters and lengths of all arteries varies with the same constant factor when iterating over these two parameters. Finally, we do not account for more complex blood vessel behavior including the cerebral auto-regulatory system (Subudhi et al., 2010) as well as vasoconstriction and vasodilation due to hypoxia (Lumb and Slinger, 2015).

5. Conclusion

In this study, we analyzed how various VA-ECMO clinician-tunable parameters influenced cerebral oxygenation. To simulate VA-ECMO flow, we developed a 1D simulator coupled to a two-phase flow model. With this model, we were able to simulate how various combinations of blood flow parameters influenced oxygenation. Our results showed a strong influence of VA-ECMO flow rates and cannula insertion locations on oxygenated blood flow to the brain, with minimal influence from blood viscosity, heart rate, SVR, and cannula position.

CRediT authorship contribution statement

Bradley Feiger: Conceptualization, Methodology, Software, Investigation, Formal analysis, Visualization, Validation, Writing - original draft. **Ajar Kochar:** Conceptualization, Writing - review & editing. **John Gounley:** Writing - review & editing, Formal analysis, Methodology. **Desiree Bonadonna:** Writing - review & editing, Resources. **Mani Daneshmand:** Conceptualization, Writing - review & editing, Resources. **Amanda Randles:** Conceptualization, Methodology, Writing - review & editing, Supervision.

Declaration of Competing Interest

The authors declare that they have no known competing financial interests or personal relationships that could have appeared to influence the work reported in this paper.

Acknowledgments

Research reported in this publication was supported by the Office of the Director, National Institutes Of Health under Award Number DP5OD019876. The content is solely the responsibility of the authors and does not necessarily represent the official views of the National Institutes of Health. Support was provided by the Big Data-Scientist Training Enhancement Program (BD-STEP) of the Department of Veterans Affairs, the Hartwell Foundation, and Duke Morton H. Friedman Fellowship. We thank Duke OIT for their help with the Duke Compute Cluster runs.

Appendix A. Supplementary material

Supplementary data associated with this article can be found, in the online version, at https://doi.org/10.1016/j.jbiomech.2020.109707.

References

Alastruey, J., Khir, A.W., Matthys, K.S., Segers, P., Sherwin, S.J., Verdonck, P.R., Parker, K.H., Peiró, J., 2011. Pulse wave propagation in a model human arterial network: assessment of 1-D visco-elastic simulations against in vitro measurements. J. Biomech. 44, 2250–2258.

Alastruey, J., Parker, K.H., Sherwin, S.J., et al., 2012. Arterial pulse wave haemodynamics. In: 11th International Conference on Pressure Surges. Virtual PiE Led t/a BHR Group Lisbon, Portugal, pp. 401–442.

Aniszewski, W., Ménard, T., Marek, M., 2014. Volume of fluid (VOF) type advection methods in two-phase flow: a comparative study. Comput. Fluids 97, 52–73.

Boileau, E., Nithiarasu, P., Blanco, P.J., Müller, L.O., Fossan, F.E., Hellevik, L.R., Donders, W.P., Huberts, W., Willemet, M., Alastruey, J., 2015. A benchmark study of numerical schemes for one-dimensional arterial blood flow modelling. Int. J. Numer. Methods Biomed. Eng. 31, e02732.

Cevasco, M., Ikegami, H., Willey, J., Garan, A., Chan, C., Han, J., Colombo, P., Yusefpolskaya, M., Kurlansky, P., Naka, Y., et al., 2018. VA-ECMO cannulation strategy and influence on cerebral blood flow velocities. J. Heart Lung Transplantat. 37, S285.

Cheng, R., Hachamovitch, R., Kittleson, M., Patel, J., Arabia, F., Moriguchi, J., Esmailian, F., Azarbal, B., 2014. Complications of extracorporeal membrane oxygenation for treatment of cardiogenic shock and cardiac arrest: a meta-analysis of 1,866 adult patients. Ann. Thoracic Surg. 97, 610–616.

Diem, A.K., Bressloff, N.W., 2017. VaMpy: a Python package to solve 1D blood flow problems. J. Open Res. Softw., 5

van Dijk, R., Nijpels, G., Twisk, J., Steyn, M., Dekker, J., Heine, R., Donker, A., Stehouwer, C., 2000. Change in common carotid artery diameter, distensibility and compliance in subjects with a recent history of impaired glucose tolerance: a 3-year follow-up study. J. Hypertens. 18, 293–300.

Eck, V.G., Donders, W.P., Sturdy, J., Feinberg, J., Delhaas, T., Hellevik, L.R., Huberts, W., 2016. A guide to uncertainty quantification and sensitivity analysis for cardiovascular applications. Int. J. Numer. Methods Biomed. Eng. 32, e02755.

ECLS registry report, 2018. Extracorporeal Life Support Organization.

Fearn, S., Pole, R., Wesnes, K., Faragher, E., Hooper, T., McCollum, C., 2001. Cerebral injury during cardiopulmonary bypass: emboli impair memory. J. Thoracic Cardiovasc. Surg. 121, 1150–1160.

Giannopoulos, A.A., Chatzizisis, Y.S., Maurovich-Horvat, P., Antoniadis, A.P., Hoffmann, U., Steigner, M.L., Rybicki, F.J., Mitsouras, D., 2016. Quantifying the effect of side branches in endothelial shear stress estimates. Atherosclerosis 251, 213–218.

Gu, K., Zhang, Y., Gao, B., Chang, Y., Zeng, Y., 2016. Hemodynamic differences between central ECMO and peripheral ECMO: a primary CFD study. Med. Sci. Monit. Int. Med. J. Exp. Clin. Res. 22, 717.

Gu, K., Zhang, Z., Gao, B., Chang, Y., Wan, F., 2018. Hemodynamic effects of perfusion level of peripheral ECMO on cardiovascular system. Biomed. Eng. Online 17, 59.

Kajishima, T., Taira, K., 2017. Finite-difference discretization of the advection-diffusion equation. In: Computational Fluid Dynamics. Springer, pp. 23–72.

Kazmi, S.O., Sivakumar, S., Karakitsos, D., Alharthy, A., Lazaridis, C., 2018. Cerebral pathophysiology in extracorporeal membrane oxygenation: pitfalls in daily clinical management. Crit. Care Res. Pract.

Kim, H.S., Ha, S.O., Yu, K.-H., Oh, M.S., Park, S., Lee, S.H., Han, S.J., Kim, H.-S., Chang, I. B., Ahn, J.H., 2019. Cerebral oxygenation as a monitoring parameter for mortality during venoarterial extracorporeal membrane oxygenation. Asaio J. 65, 342–348.

Le Guennec, L., Cholet, C., Huang, F., Schmidt, M., Bréchot, N., Hékimian, G., Besset, S., Lebreton, G., Nieszkowska, A., Leprince, P., et al., 2018. Ischemic and hemorrhagic brain injury during venoarterial-extracorporeal membrane oxygenation. Ann. Intensive Care 8, 129.

Lorusso, R., Barili, F., Mauro, M.D., Gelsomino, S., Parise, O., Rycus, P.T., Maessen, J., Mueller, T., Muellenbach, R., Belohlavek, J., et al., 2016. In-hospital neurologic complications in adult patients undergoing venoarterial extracorporeal membrane oxygenation: results from the Extracorporeal Life Support Organization Registry. Crit. Care Med. 44, e964–e972.

Lumb, A.B., Slinger, P., 2015. Hypoxic pulmonary vasoconstriction: physiology and anesthetic implications. Anesthesiology 122, 932–946.

Makdisi, G., Wang, I., 2015. Extra corporeal membrane oxygenation (ECMO) review of a lifesaving technology. J. Thoracic Dis. 7, E166.

Meani, P., Pappalardo, F., 2017. The step forward for VA ECMO: left ventricular unloading!. J. Thoracic Dis. 9, 4149.

Napp, L.C., Kühn, C., Hoeper, M.M., Vogel-Claussen, J., Haverich, A., Schäfer, A., Bauersachs, J., 2016. Cannulation strategies for percutaneous extracorporeal membrane oxygenation in adults. Clin. Res. Cardiol. 105, 283–296.

Newman, M.F., Croughwell, N.D., Blumenthal, J.A., White, W.D., Lewis, J.B., Smith, L. R., Frasco, P., Towner, E.A., Schell, R.M., Hurwitz, B.J., 1994. Effect of aging on cerebral autoregulation during cardiopulmonary bypass. Association with postoperative cognitive dysfunction. Circulation 90. II243-9.

Please cite this article as: B. Feiger, A. Kochar, J. Gounley et al., Determining the impacts of venoarterial extracorporeal membrane oxygenation on cerebral oxygenation using a one-dimensional blood flow simulator, Journal of Biomechanics, https://doi.org/10.1016/j.jbiomech.2020.109707

Olufsen, M.S., Peskin, C.S., Kim, W.Y., Pedersen, E.M., Nadim, A., Larsen, J., 2000. Numerical simulation and experimental validation of blood flow in arteries with structured-tree outflow conditions. Ann. Biomed. Eng. 28, 1281–1299.

Pavlushkov, E., Berman, M., Valchanov, K., 2017. Cannulation techniques for extracorporeal life support. Ann. Translational Med., 5

Ranney, D.N., Benrashid, E., Meza, J.M., Keenan, J.E., Bonadonna, D.K., Bartz, R., Milano, C.A., Hartwig, M.G., Haney, J.C., Schroder, J.N., et al., 2017. Central cannulation as a viable alternative to peripheral cannulation in extracorporeal membrane oxygenation. In: Seminars in Thoracic and Cardiovascular Surgery, vol. 29. Elsevier, pp. 188–195.

Sakota, D., Sakamoto, R., Sobajima, H., Yokoyama, N., Waguri, S., Ohuchi, K., Takatani, S., 2008. Mechanical damage of red blood cells by rotary blood pumps: selective destruction of aged red blood cells and subhemolytic trauma. Artif. Organs 32, 785–791.

Sherwin, S., Formaggia, L., Peiro, J., Franke, V., 2003. Computational modelling of 1D blood flow with variable mechanical properties and its application to the simulation of wave propagation in the human arterial system. Int. J. Numer. Meth. Fluids 43, 673–700.

Shi, Y., Lawford, P., Hose, R., 2011. Review of zero-D and 1-D models of blood flow in the cardiovascular system. Biomed. Eng. Online 10, 33.

Smith, N., Pullan, A., Hunter, P.J., 2002. An anatomically based model of transient coronary blood flow in the heart. SIAM J. Appl. Math. 62, 990–1018.

Smulyan, H., Marchais, S.J., Pannier, B., Guerin, A.P., Safar, M.E., London, G.M., 1998. Influence of body height on pulsatile arterial hemodynamic data. J. Am. Coll. Cardiol. 31, 1103–1109.

Sobol, I., Tarantola, S., Gatelli, D., Kucherenko, S., Mauntz, W., et al., 2007. Estimating the approximation error when fixing unessential factors in global sensitivity analysis. Reliab. Eng. Syst. Saf. 92, 957–960.

Sorokin, V., MacLaren, G., Vidanapathirana, P.C., Delnoij, T., Lorusso, R., 2017. Choosing the appropriate configuration and cannulation strategies for extracorporeal membrane oxygenation: the potential dynamic process of organ support and importance of hybrid modes. Eur. J. Heart Fail. 19, 75–83.

Squiers, J.J., Lima, B., DiMaio, J.M., 2016. Contemporary extracorporeal membrane oxygenation therapy in adults: fundamental principles and systematic review of the evidence. J. Thoracic Cardiovasc. Surg. 152, 20–32.

Stevens, M., Callaghan, F., Forrest, P., Bannon, P., Grieve, S., 2017. Flow mixing during peripheral veno-arterial extra corporeal membrane oxygenation–a simulation study. J. Biomech. 55, 64–70.

Stevens, M.C., Callaghan, F.M., Forrest, P., Bannon, P.G., Grieve, S.M., 2018. A computational framework for adjusting flow during peripheral extracorporeal membrane oxygenation to reduce differential hypoxia. J. Biomech. 79, 39–44.

Subudhi, A.W., Panerai, R.B., Roach, R.C., 2010. Effects of hypobaric hypoxia on cerebral autoregulation. Stroke 41, 641–646.

Vardhan, M., Gounley, J., Chen, S.J., Kahn, A.M., Leopold, J.A., Randles, A., 2019. The importance of side branches in modeling 3D hemodynamics from angiograms for patients with coronary artery disease. Sci. Rep. 9, 1–10.

Wang, X., 2014. 1D Modeling of Blood Flow in Networks: Numerical Computing and Applications (Ph.D. thesis). Université Pierre et Marie Curie-Paris VI.

Westerhof, N., Lankhaar, J.-W., Westerhof, B.E., 2009. The arterial Windkessel. Med. Biol. Eng. Comput. 47, 131–141.

Wildman, R.P., Mehta, V., Thompson, T., Brockwell, S., Sutton-Tyrrell, K., 2004. Obesity is associated with larger arterial diameters in caucasian and african-american young adults. Diabetes Care 27, 2997–2999.

Willemet, M., Chowienczyk, P., Alastruey, J., 2015. A database of virtual healthy subjects to assess the accuracy of foot-to-foot pulse wave velocities for estimation of aortic stiffness. Am. J. Physiol. Heart Circulatory Physiol. 309, H663–H675.

Xiao, N., Alastruey, J., Alberto Figueroa, C., 2014. A systematic comparison between 1-D and 3-D hemodynamics in compliant arterial models. Int. J. Numer. Methods Biomed. Eng. 30, 204–231.

Zhang, Q., Gao, B., Shi, Y., Yu, C., 2018. The hemodynamic comparative study between pulsatile and non-pulsatile VA ECMO: a primary numerical study. Comput. Model. Eng. Sci. 116, 247–262.

Zhong, Z.-P., Wang, H., Hou, X.-T., 2016. Extracorporeal membrane oxygenation as a bridge for heart failure and cardiogenic shock. BioMed Res. Int.

Further reading

Carson, J., Van Loon, R., 2017. An implicit solver for 1D arterial network models. Int. J. Numer. Methods Biomed. Eng. 33, e2837.

Ho, C.-H., 2004. White blood cell and platelet counts could affect whole blood viscosity. J. Chin. Med. Assoc. 67, 394–397.

Huberts, W., de Jonge, C., van der Linden, W., Inda, M., Passera, K., Tordoir, J., van de Vosse, F., Bosboom, E., 2013a. A sensitivity analysis of a personalized pulse wave propagation model for arteriovenous fistula surgery. Part B: identification of possible generic model parameters. Med. Eng. Phys. 35, 827–837.

Huberts, W., de Jonge, C., van der Linden, W., Inda, M., Tordoir, J., van de Vosse, F., Bosboom, E., 2013b. A sensitivity analysis of a personalized pulse wave propagation model for arteriovenous fistula surgery. Part A: identification of most influential model parameters. Med. Eng. Phys. 35, 810–826.

Laskey, W.K., Parker, H.G., Ferrari, V.A., Kussmaul, W.G., Noordergraaf, A., 1990. Estimation of total systemic arterial compliance in humans. J. Appl. Physiol. 69, 112–119.

Matsuda, T., Murakami, M., 1976. Relationship between fibrinogen and blood viscosity. Thromb. Res. 8, 25–33.

Mynard, J., Nithiarasu, P., 2008. A 1D arterial blood flow model incorporating ventricular pressure, aortic valve and regional coronary flow using the locally conservative Galerkin (LCG) method. Commun. Numer. Methods Eng. 24, 367–417.

Napp, L., Kühn, C., Bauersachs, J., 2017. ECMO in cardiac arrest and cardiogenic shock. Herz 42, 27–44.

Pappalardo, F., Pieri, M., Corada, B.A., Ajello, S., Melisurgo, G., De Bonis, M., Zangrillo, A., 2015. Timing and strategy for weaning from venoarterial ECMO are complex issues. J. Cardiothorac. Vasc. Anesth. 29, 906–911.

Pirofsky, B., 1953. The determination of blood viscosity in man by a method based on Poiseuille's law. J. Clin. Investig. 32, 292–298.

Rosenblum, W., Asofsky, R., 1967. Effects of dehydration on blood viscosity and on distribution of plasma proteins in experimental macroglobulinaemia. Nature 216, 1327.

Ruggiero, H., Castellanos, H., Caprissi, L., Caprissi, E., 1982. Heparin effect on blood viscosity. Clin. Cardiol. 5, 215–218.

Tariq, S., Aronow, W., 2015. Use of inotropic agents in treatment of systolic heart failure. Int. J. Mol. Sci. 16, 29060–29068.

Please cite this article as: B. Feiger, A. Kochar, J. Gounley et al., Determining the impacts of venoarterial extracorporeal membrane oxygenation on cerebral oxygenation using a one-dimensional blood flow simulator, Journal of Biomechanics, https://doi.org/10.1016/j.jbiomech.2020.109707